Liquidus Projection and Isothermal Section of the Sb-Se-Sn System

JUI-SHEN CHANG and SINN-WEN CHEN

Sb-Se-Sn ternary alloys are promising chalcogenide materials. The liquidus projection and 673.2 K (400 °C) isothermal section of the Sb-Se-Sn ternary system are determined. Numerous Sb-Se-Sn alloys are prepared, and their primary solidification phases are examined. In addition to the three terminal phases, (Sb), (Se) and (Sn), there are Sb_2Sn_3, SbSn, SnSe, $SnSe_2$, Sb_2Se_3, $Sn_2Sb_9Se_9$, and $SnSb_2Se_4$ phases. In addition, there are two miscibility gaps along the Sb-Se and Se-Sn and sides. There are ten invariant reactions in the Sb-Se-Sn ternary system, and seven of them are experimentally determined in this study. The lowest reaction temperature of determined invariant reaction is L + SbSn = (Sn) + SnSe at 515.4 K ± 5 K (242.2 °C ± 5 °C). There are nine tie-triangles, which are Liquid + SbSn + SnSe, SbSn + SnSe + (Sb), SnSe + (Sb) + $Sn_2Sb_9Se_9$, (Sb) + Sb_2Se_3 + $Sn_2Sb_9Se_9$, SnSe + $Sn_2Sb_9Se_9$ + $SnSb_2Se_4$, Sb_2Se_3 + $Sn_2Sb_9Se_9$ + $SnSb_2Se_4$, SnSe + $SnSe_2$ + $SnSb_2Se_4$, $SnSe_2$ + $SnSb_2Se_4$ + Sb_2Se_3, and $SnSe_2$ + Sb_2Se_3 + Liquid in the 673.2 K (400 °C) isothermal section of the Sb-Se-Sn ternary system.

DOI: 10.1007/s40553-017-0110-8

I. INTRODUCTION

CHALCOGENIDE glasses have attracted intensive research interest recently due to their potential electrical, optical, and energy applications.[1–13] Numerous types of chalcogenide materials have been proposed, including Sb-Se-Sn (TAS), Sb-Se-Sn-Te, Sb-Se-Sn-Bi, and Cu-Sb-Se-Sn alloys.[1–13] Sb-Se and Sn-Se alloys are promising solar cell materials, especially the Sb_2Se_3, SnSe, and $SnSe_2$ compounds.[14–18] Moreover, the Sb-Se-Sn system is a promising absorber material system for solar cells applications.[8,10]

Nevertheless, there is relatively little phase-equilibrium data for the Sb-Se-Sn system in the literature.[19,20] The phase diagrams of its three constituent binary systems, Sn-Sb, Sn-Se, and Sb-Se, have been examined.[21–23] The SnSe-Sb_2Se_3 and SnSe-(Sb) isoplethal sections have been determined.[19,20] Three ternary compounds, $SnSb_2Se_4$, $Sn_2Sb_6Se_{11}$, and $Sn_2Sb_2Se_5$, are found in the literature.[24–27] However, there are no available isothermal sections and liquidus projection of the Sb-Se-Sn ternary system.

Phase diagrams are important tools for understanding materials development and materials process routes. This study thus determines the liquidus projection and isothermal section at 673.2 K (400 °C) of the Sb-Se-Sn system. The Sb-Se-Sn ternary alloys are prepared, and their primary solidification phases, temperature of invariant reactions, and isothermal section at 673.2 K (400 °C) are proposed based on the above-mentioned ternary experimental data and its three constituent systems, Sn-Sb, Sn-Se, and Sb-Se.[21–23]

II. EXPERIMENTAL PROCEDURES

Proper amounts of pure Sn (99.99 wt pct, Alfa Aesar, Ward Hill, MA), Sb (99.9999 wt pct, Alfa Aesar, Ward Hill, MA), and Se (99.999 wt pct, Alfa Aesar, Ward Hill, MA) with a total weight of one gram were weighed and encapsulated in a quartz tube in a 2×10^{-5} bar vacuum. The alloys were prepared with extra care due to the high vapor pressure of Se. The sample capsules of alloys with Se contents lower than 50 atomic percent were placed in a furnace at room temperature, heated slowly to 1273.2 K (1000 °C) at a rate of 15 K/h (15 °C/h), homogenized at 1273.2 K (1000 °C) for one day, and then quenched in water. The maximum and homogenization temperature was 1123.2 K (850 °C) for the alloys with Se contents higher than 50 atomic percent. To determine the liquidus projection, the as-solidified alloy ingot was cut into halves. For the isothermal section determination, the quenched alloy was equilibrated at 673.2 K (400 °C) for six months, and then the alloy was also cut into halves. One half of each was mounted, polished, and metallographically analyzed,

JUI-SHEN CHANG and SINN-WEN CHEN are with the Department of Chemical Engineering, National Tsing Hua University, #101, Sec. 2, Kuang-Fu Road, 300, Hsinchu, Taiwan. Contact e-mail: swchen@mx.nthu.edu.tw

Manuscript submitted January 31, 2017
Article published online July 25, 2017

Table I. Compositions and Primary Solidification Phases of the Sn-Sb-Se Alloys Examined

Alloy #	Nominal Composition Sn (At. Pct)	Sb (At. Pct)	Se (At. Pct)	Primary Solidification Phase	Alloy #	Nominal Composition Sn (At. Pct)	Sb (At. Pct)	Se (At. Pct)	Primary Solidification Phase
1	80.0	10.0	10.0	SnSe	23	20.0	60.0	20.0	SnSe
2	75.0	20.0	5.0		24	10.0	80.0	10.0	
3	72.0	4.0	24.0		25	5.0	90.0	5.0	
4	70.0	10.0	20.0		26	35.0	2.0	63.0	$SnSe_2$
5	70.0	20.0	10.0		27	2.0	83.0	15.0	(Sb)
6	67.5	29.5	3.0		28	2.0	93.0	5.0	
7	65.0	2.0	33.0		29	10.0	55.0	35.0	miscibility gap
8	60.0	10.0	30.0		30	10.0	60.0	30.0	
9	60.0	20.0	20.0		31	5.0	60.0	35.0	
10	55.0	43.0	2.0		32	5.0	65.0	30.0	
11	50.0	10.0	40.0		33	5.0	70.0	25.0	
12	50.0	30.0	20.0		34	15.0	35.0	50.0	$Sn_2Sb_9Se_9$
13	40.0	20.0	40.0		35	10.0	35.0	55.0	
14	40.0	30.0	30.0		36	10.0	40.0	50.0	
15	40.0	50.0	10.0		37	5.0	40.0	55.0	
16	30.0	10.0	60.0		38	5.0	45.0	50.0	
17	30.0	30.0	40.0		39	20.0	20.0	60.0	$SnSb_2Se_4$
18	25.0	25.0	50.0		40	15.0	25.0	60.0	
19	23.0	29.0	48.0		41	2.5	27.5	70.0	Sb_2Se_3
20	20.0	30.0	50.0		42	5.0	30.0	65.0	
21	18.0	34.0	48.0		43	2.5	37.5	60.0	
22	20.0	50.0	30.0						

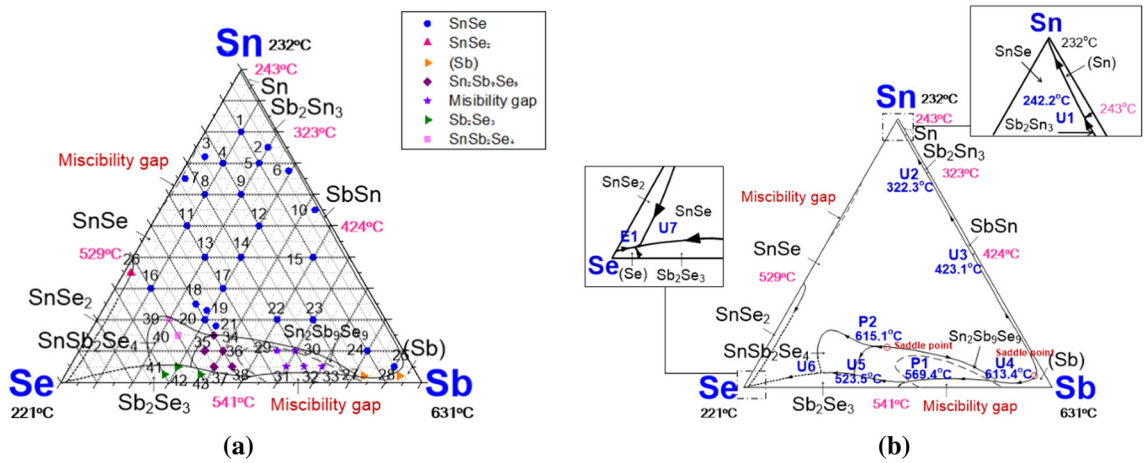

Fig. 1—(*a*) The forty-three Sn-Sb-Se ternary alloys examined in this study superimposed on the Sn-Sb-Se liquidus projection. (*b*) The liquidus projection of Sn-Sb-Se ternary system.

and the other half was used for X-ray diffraction analysis (XRD) and differential thermal analysis (DTA).

Microstructures of the samples and compositions of the phases were determined using scanning electron microscopy (SEM, Hitachi, S-2500, Japan) and electron probe microanalysis (EPMA, JEOL, JXA-8600SX, Japan). Pure Sn, Sb and Se were used for the standard atomic number, absorption and characteristic fluorescence correction (ZAF) to compute the intensities of Sn-Lα, Sb-Lα, and Se-Kα to concentrations.[28] The uncertainty of the EPMA measurement is around 3 pct of the measured values. An X-ray powder diffractometer (MAC Science, Scintac, XDS-2000 V/H) was used for XRD, with Cu-kα being the radiation source and a scanning rate of 2 deg/min. A Perkin-Elmer DTA (DTA 7, Perkin Elmer) was used to determine the reaction temperatures of the invariant reactions and the solidification paths.

III. RESULTS AND DISCUSSIONS

A. *Determination of Univariant Lines of Liquidus Projection*

The liquidus projection contains information regarding univariant lines and invariant reactions. The univariant lines delineate the boundaries of different

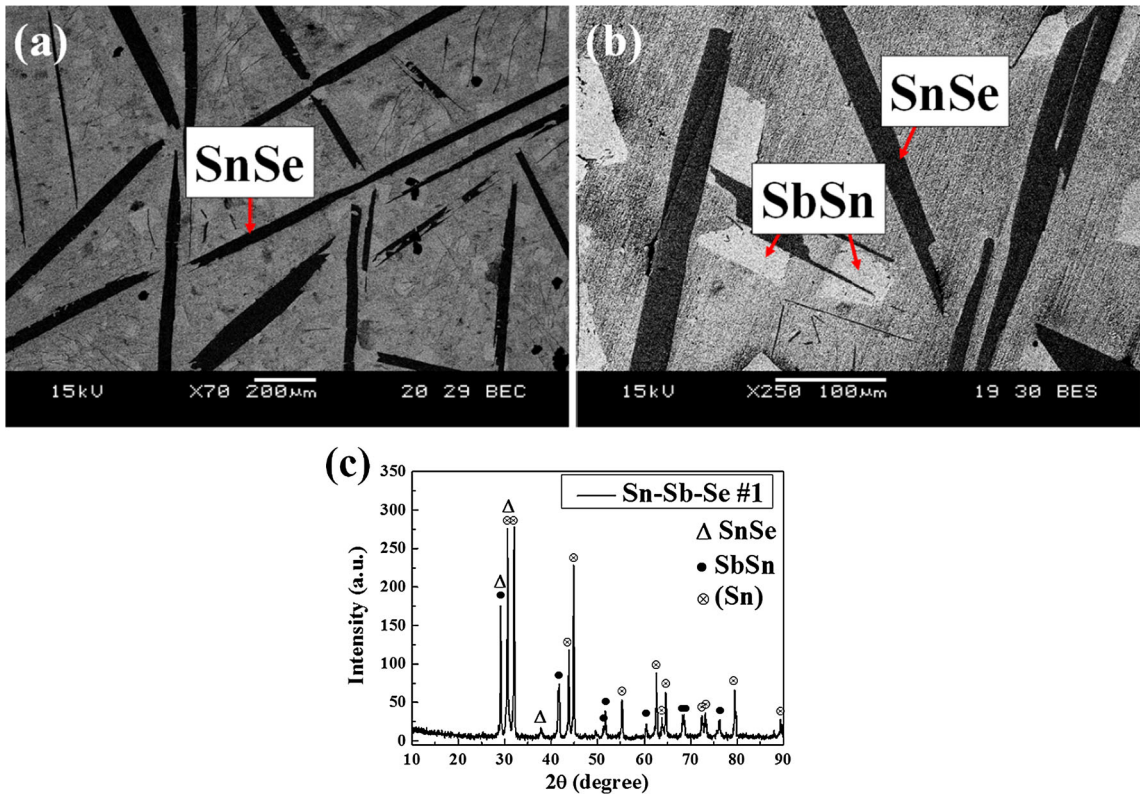

Fig. 2—(*a*) The BEI micrograph of the as-solidified alloy #1 (Sn-10.0 at. pct Sb-10.0 at. pct Se) showing the SnSe primary solidification phase. (*b*) The higher-magnification BEI micrograph of the as-solidified alloy #1. (*c*) The XRD diffractogram of the as-solidified alloy #1.

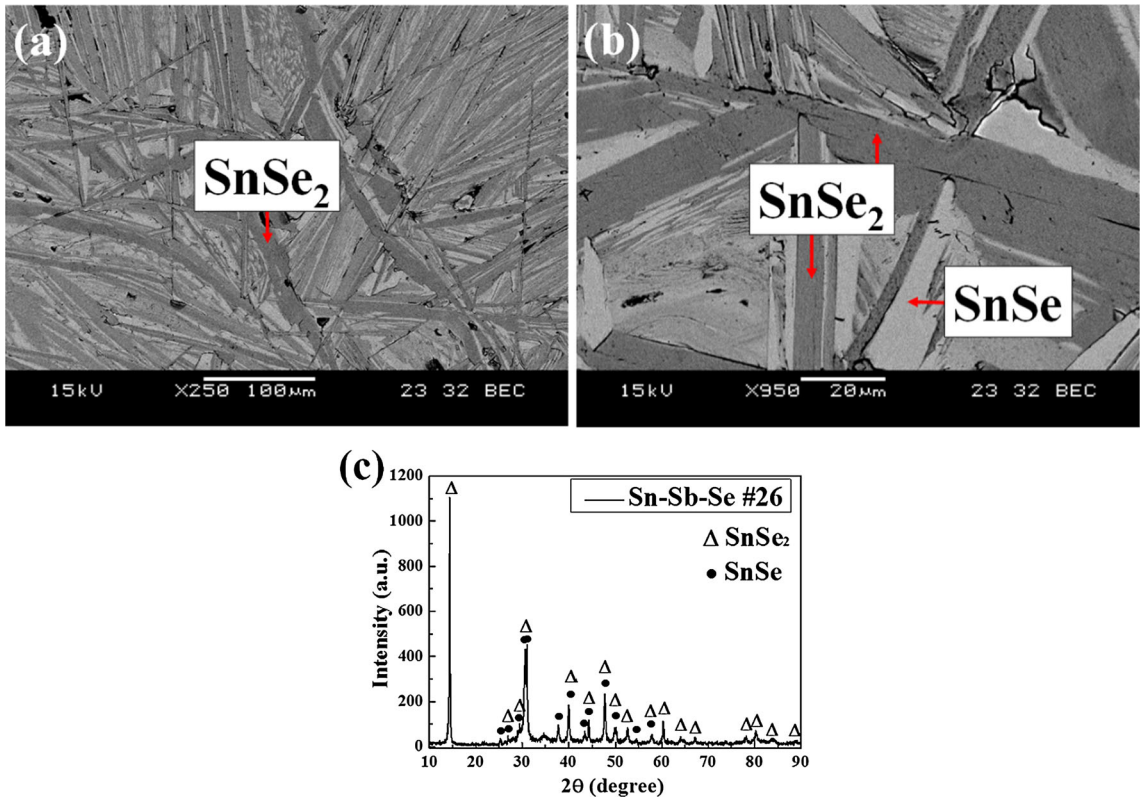

Fig. 3—(*a*) The BEI micrograph of the as-solidified alloy #26 (Sn-2.0 at. pct Sb-63.0 at. pct Se) showing the $SnSe_2$ primary solidification phase. (*b*) The higher-magnification BEI micrograph of the as-solidified alloy #26. (*c*) The XRD diffractogram of the as-solidified alloy #26.

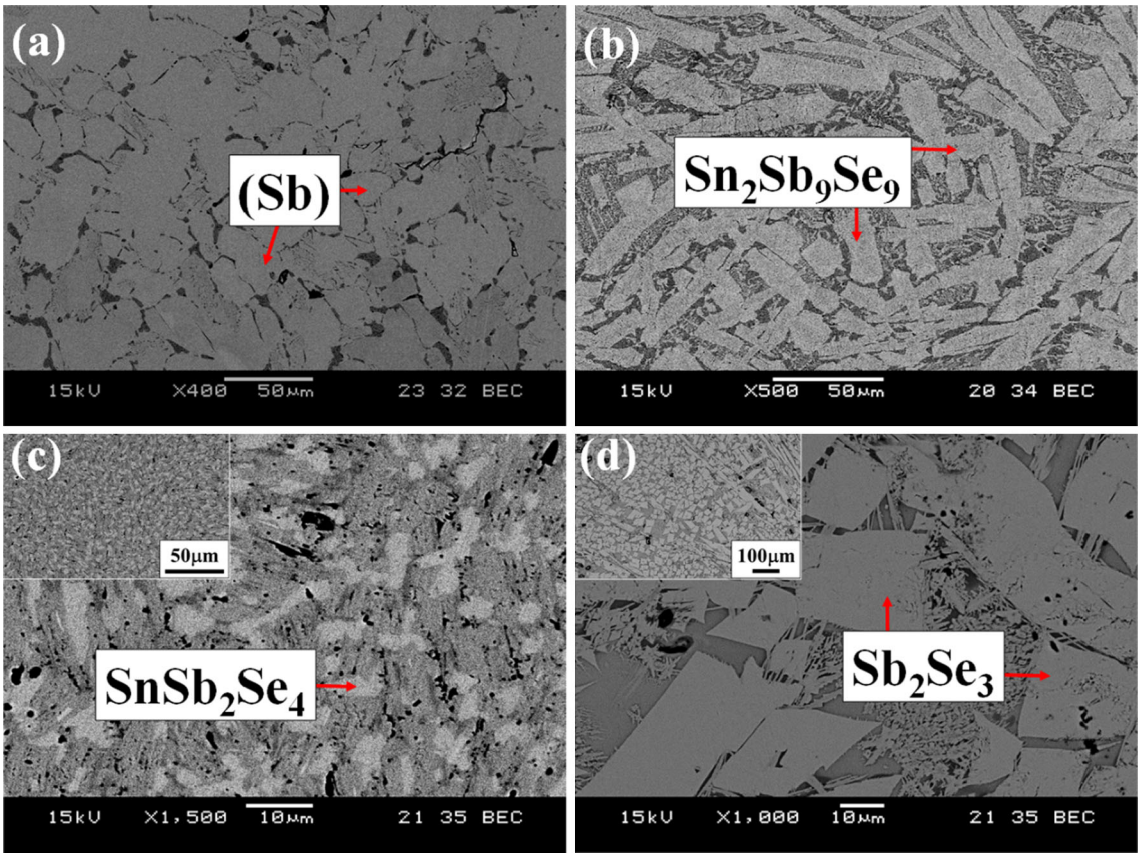

Fig. 4—(*a*) The BEI micrograph of the as-solidified alloy #28 (Sn-93.0 at. pct Sb-5.0 at. pct Se) showing the (Sb) primary solidification phase. (*b*) The BEI micrograph of the as-solidified alloy #36 (Sn-40.0 at. pct Sb-50.0 at. pct Se) showing the $Sn_2Sb_9Se_9$ primary solidification phase. (*c*) The BEI micrograph of the as-solidified alloy #39 (Sn-20.0 at. pct Sb-60.0 at. pct Se) showing the $SnSb_2Se_4$ primary solidification phase. (*d*) The BEI micrograph of the as-solidified alloy #42 (Sn-30.0 at. pct Sb-65.0 at. pct Se) showing the Sb_2Se_3 primary solidification phase.

primary solidification phases, and the data of the primary solidification phase can thus be used to construct univariant lines.[29–32] The primary solidification phase is the first phase that solidified from the liquid during the solidification path, and it can be determined by the as-solidified microstructures since they are larger, and have more complete shape and adherence than other phases. Forty-three Sb-Se-Sn alloys were prepared for determining the liquidus projection of the Sb-Se-Sn ternary system, and their nominal compositions are listed in the Table I. Figures 1(a) and (b) show the Sb-Se-Sn liquidus projection with and without superimpositions of the forty-three Sb-Se-Sn ternary alloys, respectively.

Figures 2(a) and (b) show the backscattered electron images (BEI) micrograph of the as-solidified alloy #1 (Sn-10.0 at. pct Sb-10.0 at. pct Se). According to the low-magnification image shown in Figure 2(a), the black platy phase with complete shape can be determined as the primary solidification of alloy #2. From the higher-magnification image shown in Figure 2(b), the small bright bulk phase adhered with black platy phase can be found, which can be determined as the secondary solidification phase solidified after primary solidification phase. The composition of black platy phase is Sn-49.6 at. pct Se, which can be determined as the SnSe phase from the Sn-Se binary phase diagram.[22] Furthermore, the bright bulk phase can be found from the microstructure, and its composition is Sn-52.3 at. pct Sb-0.5 at. pct Se, which is SbSn phase.[21] It needs mentioning that SbSn is not a line compound and has a compositional homogeneity of 13 at. pct at 596.2 K (323 °C).[21] Figure 2(c) shows the XRD diffractogram of the as-solidified alloy #1. The diffraction peaks of the SnSe, SbSn, and (Sn) can be observed, which are in agreement with the microstructure and compositional analysis. Similar results can be investigated from the results of alloys #2 (Sn-20.0 at. pct Sb-5.0 at. pct Se)-#25 (Sn-90.0 at. pct Sb-5.0 at. pct Se), and their primary solidification phases are the SnSe phase.

The micrographs of the as-solidified alloy #26 (Sn-2.0 at. pct Sb-63.0 at. pct Se) are shown in Figures 3(a) and (b). According to the low-magnification micrograph shown in Figure 3(a), the gray platy phase located in the middle position can be determined as the primary solidification phase of alloy #26. Further, the bright platy phase surrounding gray phase is the secondary phase in higher-magnification image shown in Figure 3(b).The composition of the gray platy phase is Sn-65.1 at. pct Se, which is the $SnSe_2$ phase. The composition of the bright phase is Sn-1.3 at. pct Sb-47.9 at. pct Se, and is the SnSe phase. Figure 3(c)

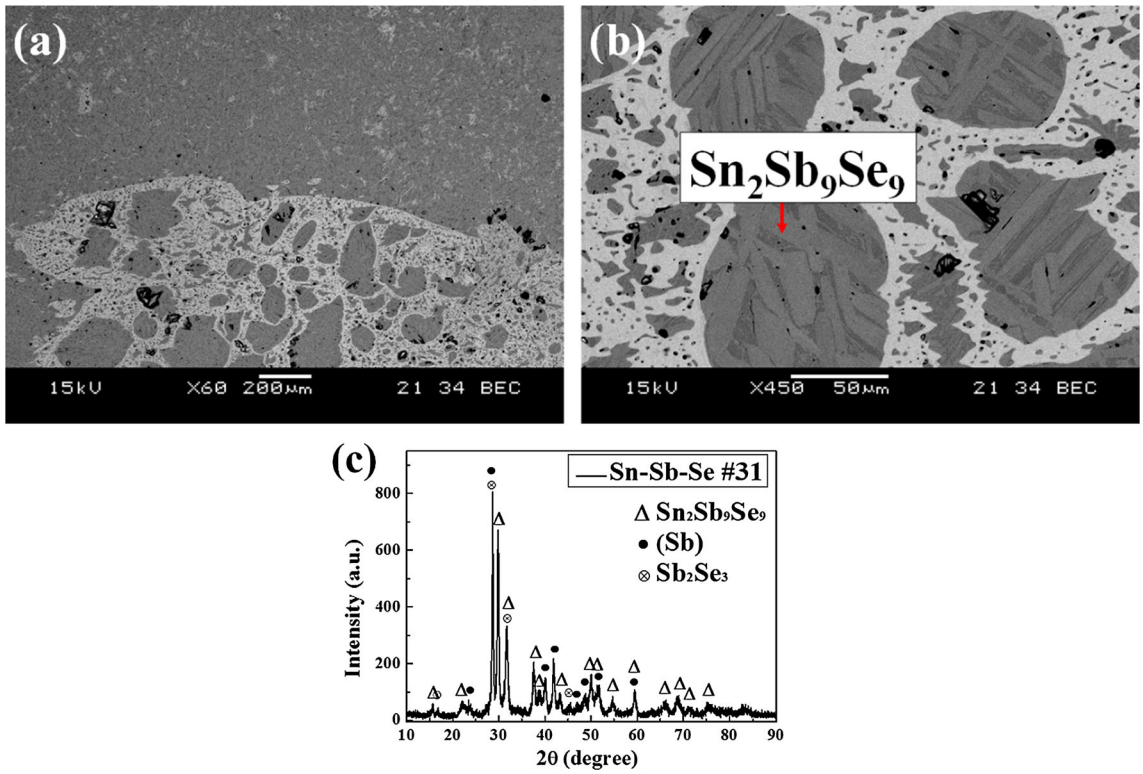

Fig. 5—(*a*) The BEI micrograph of the miscibility gap microstructure of the alloy #31 (Sn-60.0 at. pct Sb-35.0 at. pct Se) showing the $Sn_2Sb_9Se_9$ primary solidification phase. (*b*) Close-up of the mush zone portion of the miscibility gap microstructure of the as-solidified alloy #31. (*c*) The XRD diffractogram of the as-solidified alloy #31.

shows the XRD diffractogram of the as-solidified alloy #26, and the diffraction peaks of $SnSe_2$ and SnSe can be observed.

Figures 4(a) through (d) show the BEI micrographs of alloys #28 (Sn-93.0 at. pct Sb-5.0 at. pct Se), #36 (Sn-40.0 at. pct Sb-50.0 at. pct Se), #39 (Sn-20.0 at. pct Sb-60.0 at. pct Se), and #42 (Sn-30.0 at. pct Sb-65.0 at. pct Se). Following similar analytical procedures, the primary solidification phases for alloys #28, #36, #39, and #42 can be determined as bright bulk phase (#28), gray chunky phase (#36), gray bulk phase (#39), and bright chunky phase (#42). Their compositions are Sn-98.7 at. pct Sb, Sn-44.8 at. pct Sb-43.7 at. pct Se, Sn-29.3 at. pct Sb-56.1 at. pct Se, and Sn-40.3 at. pct Sb-57.9 at. pct Se, which are (Sb), $Sn_2Sb_9Se_9$, $SnSb_2Se_4$, and Sb_2Se_3 phases, respectively.

Figure 5(a) shows the BEI micrograph of the as-solidified alloy #31 (Sn-60.0 at. pct Sb-35.0 at. pct Se). Based on the BEI image, the clear phase-separation phenomenon can be investigated. The microstructure can be divided into two different matrices, which are the darker and brighter continuous phase regions. The darker droplet-like phases are spread throughout the white matrix phase. The primary solidification phase in the darker droplet-like phase is the $Sn_2Sb_9Se_9$ phase, and its composition is Sn-43.8 at. pct Sb-45.1 at. pct Se. Figure 5(b) shows a close-up of the dark droplet. Figures 5(a) and (b) indicate that alloy #31 is located in the miscibility gap. During solidification, the two liquids solidify with different solidification results. The Se-rich liquid encounters the $Sn_2Sb_9Se_9$/(Sb) univariant line in the beginning of solidification, and the remaining liquid moves toward the Se-rich corner and encounters the invariant reaction of Liquid + (Sb) + $Sn_2Sb_9Se_9$ = Sb_2Se_3; the (Sb), $Sn_2Sb_9Se_9$, and Sb_2Se_3 phases solidify together. The Sb-rich liquid directly moves to another invariant reaction of Liquid + SnSe = (Sb) + $Sn_2Sb_9Se_9$; the (Sb), SnSe, and $Sn_2Sb_9Se_9$ ternary phases solidify. However, the SnSe phase is too small to be observed from the micrograph. Figure 5(c) shows the XRD diffractogram of the as-solidified alloy #31, and the diffraction peaks of (Sb), $Sn_2Sb_9Se_9$, and Sb_2Se_3 phases are observed. In addition to alloy #31, alloys #29 (Sn-55.0 at. pct Sb-35.0 at. pct Se), #30 (Sn-60.0 at. pct Sb-30.0 at. pct Se), #32 (Sn-65.0 at. pct Sb-30.0 at. pct Se), and #33 (Sn-70.0 at. pct Sb-25.0 at. pct Se) are also located in the miscibility gap.

To establish the univariant line of the Sb-Se-Sn liquidus projection, the binary phase diagrams of Sn-Sb, Sn-Se, and Sb-Se systems and the above-mentioned experimental results are taken into account.[21–23] From the Sn-Sb phase diagram, it is observed there are four primary solidification phase regimes, which are the (Sb), SbSn, Sb_2Sn_3, and (Sn) phases, and the boundaries of (Sb)/SbSn, SbSn/Sb_2Sn_3, and Sb_2Sn_3/(Sn) are Sn-49.5 at. pct Sb, Sn-18.5 at. pct Sb, and Sn-6.2 at. pct Sb, respectively.[21] Along the Sn-Se binary side, there are also four primary solidification phase regimes, which are the (Sn), SnSe, $SnSe_2$, and (Se) phases, respectively. According to the binary phase diagram,[22] there are two

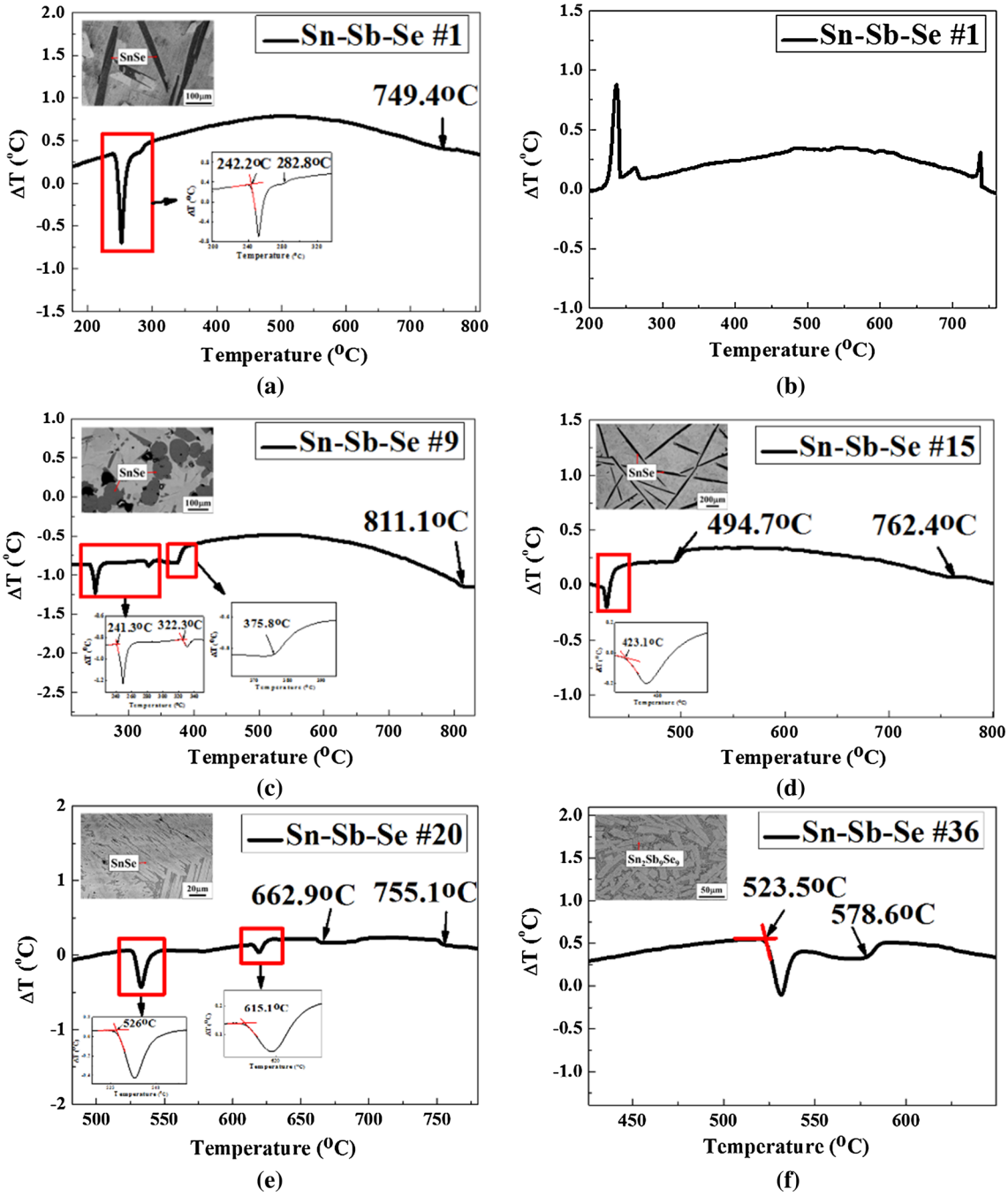

Fig. 6—(*a*) DTA heating and curves of alloy #1 at 10 K/min (10 °C/min) scanning rate. (*b*) DTA cooling and curves of alloy #1 at 10 K/min (10 °C/min) scanning rate. (*c*) DTA heating and curves of alloy #9 (Sn-20.0 at. pct Sb-20.0 at. pct Se) at 10 K/min (10 °C/min) scanning rate. (*d*) DTA heating and curves of alloy #15 (Sn-50.0 at. pct Sb-10.0 at. pct Se) at 10 K/min (10 °C/min) scanning rate. (*e*) DTA heating and curves of alloy #20 (Sn-30.0 at. pct Sb-50.0 at. pct Se) at 10 K/min (10 °C/min) scanning rate. (*f*) DTA heating and curves of alloy #36 (Sn-40.0 at. pct Sb-50.0 at. pct Se) at 10 K/min (10 °C/min) scanning rate.

SnSe phases, α-SnSe and β-SnSe, in the Sn-Se system. However, no distinction can be made between the α-SnSe and β-SnSe primary solidification phases, so this study assumes that there is only one SnSe phase. As such, the univariant reaction of β-SnSe = α-SnSe + Liquid at. 799.5 K (526.3 °C) has not been taken into account in this study. The boundary of the SnSe/$SnSe_2$ is Sn-61.3 at. pct Se. The boundaries of (Sn)/SnSe and $SnSe_2$/(Se) are hard to recognize due to the extremely low Se solubility in the (Sn) phase and low Sn solubility in (Se) phase. Further, there is a miscibility gap located near Sn-rich corner, and its compositional range is from Sn-24.0 at. pct Se to Sn-43.0 at. pct Se.[22] Finally, along the Sb-Se binary side, the boundary of Sb_2Se_3/(Sb) is Sb-50.0 at. pct Se, and the compositional range of the miscibility gap is from Sb-17.0 at. pct Se to Sb-43.0

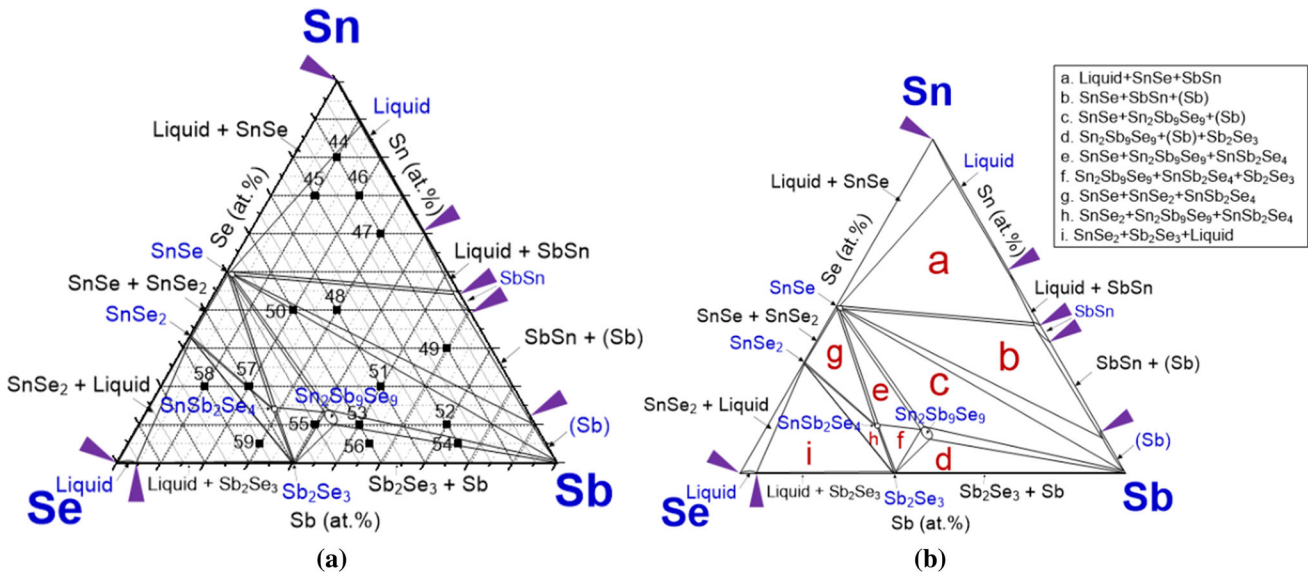

Fig. 7—(*a*) Compositions of ternary Sn-Sb-Se alloys examined in this study superimposed on the Sn-Sb-Se 673.2 K (400 °C) phase equilibria isothermal section. (*b*) 673.2 K (400 °C) phase equilibria isothermal section of Sn-Se-Sb ternary system.

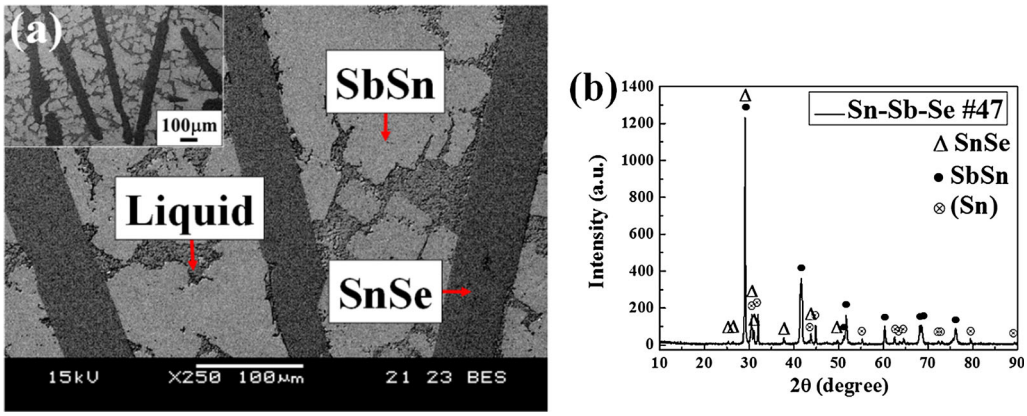

Fig. 8—(*a*) The BEI micrograph of equilibrated alloy #47 (Sn-30.0 at. pct Sb-10.0 at. pct Se). (*b*) The XRD diffractogram of equilibrated alloy #47.

Table II. Invariant Reaction Temperatures in the Sn-Sb-Se System

Reaction	Temperature (°C)
Liquid + Sb_2Sn_3 = SnSe + (Sn)	242.2 (515.4 K)
Liquid + SbSn = SnSe + Sb_2Sn_3	322.3 (595.5 K)
Liquid + (Sb) = SbSn + SnSe	423.1 (696.3 K)
Liquid + $Sn_2Sb_9Se_9$ = $SnSb_2Se_4$ + Sb_2Se_3	523.5 (796.7 K)
Liquid + $Sn_2Sb_9Se_9$ + (Sb) = Sb_2Se_3	569.4 (842.6 K)
Liquid + SnSe = (Sb) + $Sn_2Sb_9Se_9$	613.4 (886.6 K)
Liquid + $Sn_2Sb_9Se_9$ + SnSe = $SnSb_2Se_4$	615.1 (888.3 K)

at. pct Se.[23] The determined univariant lines in this study are shown in Figures 1(a) and (b), and there are ten primary solidification phase regimes in the Sb-Se-Sn ternary system, which are (Sn), (Sb), (Se), SbSn, Sb_2Sn_3, SnSe, $SnSe_2$, Sb_2Se_3, $Sn_2Sb_9Se_9$, and $SnSb_2Se_4$ phases. In addition, there are two miscibility gaps along Sn-Se and Sb-Se sides, respectively.

B. *Determination of Invariant Reaction Temperatures*

There are ten invariant reactions involving liquid in the Sb-Se-Sn ternary system as shown in Figures 1(a) and (b). Based on the results of thermal analysis, the temperatures of the invariant reactions and the temperature descending directions of the liquidus lines are determined. The methodology regarding preparations of DTA samples and determinations of invariant reaction temperatures have been described previously.[33–35] Figures 6(a) and (b) show the heating curve and cooling curve of alloy #1 at 10 K/min (10 °C/min) scanning rate, respectively. Three peaks are observed in both curves. According to the liquidus projection of the Sb-Se-Sn ternary system shown in Figure 1(b), the first peak is a heating-effect result of SnSe primary

Table III. Equilibrium Phases of Sn-Sb-Se Alloys at 673.2 K (400 °C)

	Nominal composition (At. Pct)				Composition (At. Pct)		
No.	Sn	Sb	Se	Equilibria Phase	Sn	Sb	Se
#44	80.0	10.0	10.0	liquid	87.2	12.3	0.5
				SnSe	49.5	—	50.5
				SbSn	44.2	54.8	1.0
#45	70.0	10.0	20.0	liquid	86.3	13.4	0.3
				SnSe	51.0	—	49.0
				SbSn	43.8	55.5	0.7
#46	70.0	20.0	10.0	liquid	88.3	11.5	0.2
				SnSe	50.6	0.1	49.3
				SbSn	44.1	54.7	1.2
#47	60.0	30.0	10.0	liquid	88.7	11.2	0.1
				SnSe	50.7	—	49.3
				SbSn	44.4	54.3	1.3
#48	40.0	30.0	30.0	SnSe	50.3	1.2	48.5
				SbSn	44.2	54.2	1.6
				(Sb)	10.1	89.5	0.4
#49	30.0	60.0	10.0	SnSe	49.5	0.7	49.8
				SbSn	45.7	53.0	1.3
				(Sb)	9.5	90.1	0.4
#50	40.0	20.0	40.0	SnSe	49.0	1.8	49.2
				(Sb)	2.3	97.6	0.1
#51	20.0	50.0	30.0	SnSe	50.5	1.3	48.2
				$Sn_2Sb_9Se_9$	12.1	43.1	44.8
				(Sb)	0.8	99.2	—
#52	10.0	70.0	20.0	SnSe	48.5	1.7	49.8
				$Sn_2Sb_9Se_9$	12.7	42.1	45.2
				(Sb)	1.2	98.6	0.2
#53	10.0	50.0	40.0	$Sn_2Sb_9Se_9$	11.5	44.8	43.7
				(Sb)	0.3	99.1	0.6
#54	5.0	75.0	20.0	$Sn_2Sb_9Se_9$	11.2	45.0	43.8
				(Sb)	0.7	99.3	—
#55	10.0	40.0	50.0	$Sn_2Sb_9Se_9$	13.5	41.5	45.0
				Sb_2Se_3	0.2	41.0	58.8
#56	5.0	55.0	40.0	$Sn_2Sb_9Se_9$	10.3	45.6	44.1
				(Sb)	0.6	99.2	0.2
				Sb_2Se_3	0.7	40.2	59.1
#57	20.0	20.0	60.0	$SnSe_2$	33.4	1.7	64.9
				$SnSb_2Se_4$	14.2	30.8	55.0
#58	20.0	10.0	70.0	$SnSe_2$	34.0	0.1	65.9
				Sb_2Se_3	0.3	41.0	58.7
				liquid	0.4	2.2	97.4
#59	5.0	30.0	65.0	$SnSe_2$	33.8	—	66.2
				Sb_2Se_3	0.2	41.5	58.3
				liquid	1.7	1.5	96.8

solidification phase. To obey the mass balance requirement, the remaining liquid moves away from SnSe phase and intercepts with the SnSe/Sb_2Sn_3 univariant line. The SnSe and Sb_2Sn_3 phases solidify together. The compositions of the liquid phase change following the SnSe/Sb_2Sn_3 univariant line with the lowering temperatures, and the liquid completely solidifies at the invariant reaction involving the Liquid, SnSe, Sb_2Sn_3, and (Sn) phases. The natures of the three reactions as shown in Figures 6(a) and (b) can thus be understood based on the Sb-Se-Sn liquidus projection as mentioned above, and these three peaks thus correspond to the primary phase solidification, the univariant reaction, and the invariant reaction, respectively. Due to possible undercooling,[34,35] the reaction temperatures are thus determined from the heating curve, and are 1022.6 K, 556.0 K, and 515.4 K (749.4 °C, 282.8 °C, and 242.2 °C), respectively.

Figures 6(c) through (f) show the DTA heating curves of alloys #9 (Sn-20.0 at. pct Sb- 20.0 at. pct Se), #15 (Sn-50.0 at. pct Sb-10.0 at. pct Se), #20 (Sn-30.0 at. pct Sb-50.0 at. pct Se) and #36, respectively. Following similar analytical procedures, the temperatures of these invariant reactions are determined and are summarized in Table II. As the liquidus projection shows, there are ten invariant reactions in the Sb-Se-Sn ternary system. However, since the high Se vapor pressure causes experimental difficulties, temperature of three invariant

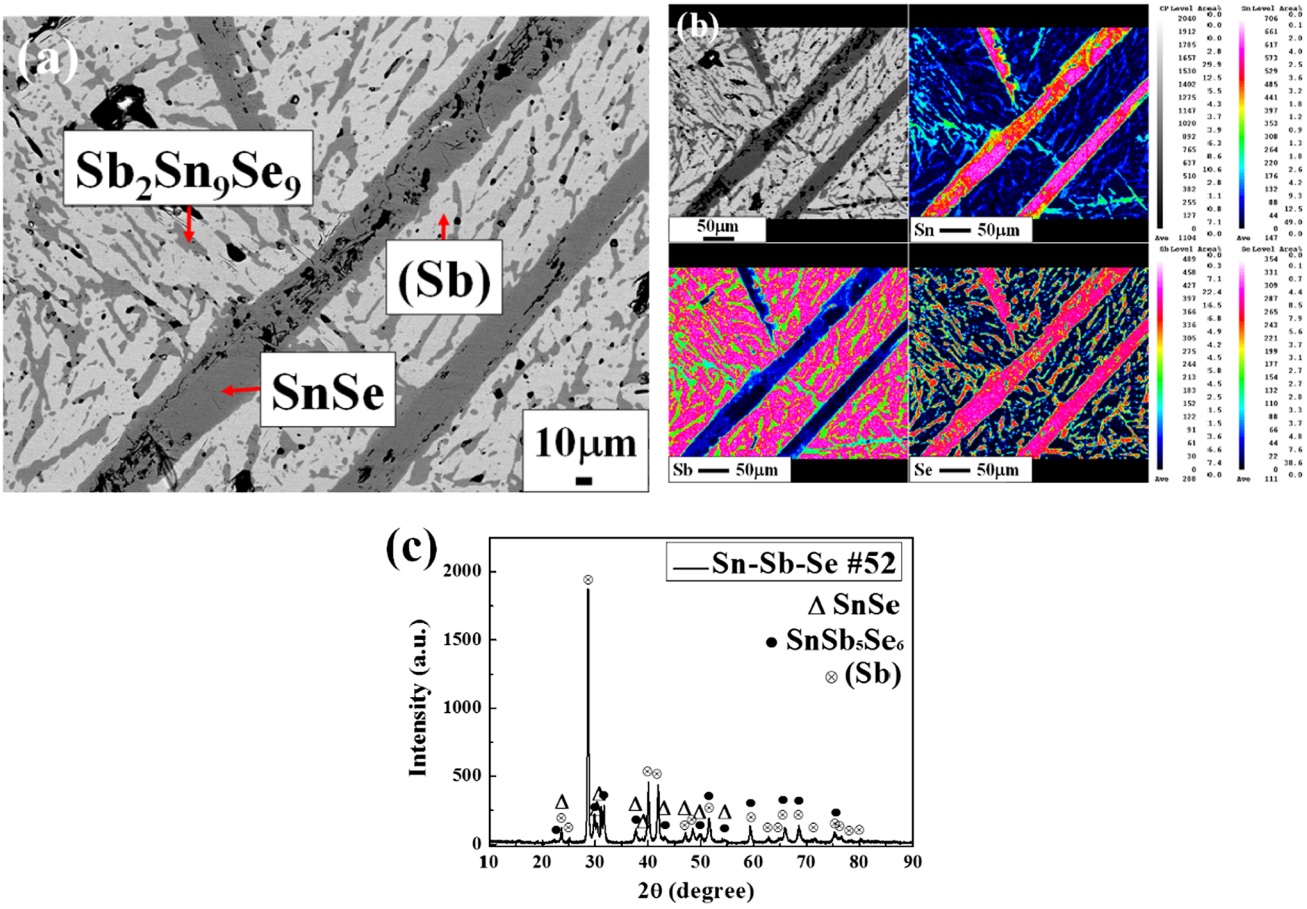

Fig. 9—(*a*) The BEI micrograph of equilibrated alloy #52 (Sn-70.0 at. pct Sb-20.0 at. pct Se). (*b*) The elemental mapping results of equilibrated alloy #52. (*c*) The XRD diffractogram of equilibrated alloy #52.

reactions located at the Se-rich corner, which are Liquid + $SnSb_2Se_4$ = SnSe + Sb_2Se_3, Liquid + SnSe = $SnSe_2$ + Sb_2Se_3, and Liquid = $SnSe_2$ + Sb_2Se_3 + (Se), have not been resolved. There are five class II reaction, Liquid + Sb_2Sn_3 = SnSe + (Sn), Liquid + SbSn = SnSe + Sb_2Sn_3, Liquid + (Sb) = SbSn + SnSe, Liquid + SnSe = (Sb) + $Sn_2Sb_9Se_9$, and Liquid + $Sn_2Sb_9Se_9$ = $SnSb_2Se_4$ + Sb_2Se_3, and two class III reactions, Liquid + $Sn_2Sb_9Se_9$ + (Sb) = Sb_2Se_3 and Liquid + $Sn_2Sb_9Se_9$ + SnSe = $SnSb_2Se_4$. Their temperatures are 515.4 K, 595.5 K, 696.3 K, 796.7 K, 842.6 K, 886.6 K, 888.3 K (242.2 °C, 322.3 °C, 423.1 °C, 523.5 °C, 569.4 °C, 613.4 °C, and 615.1 °C). It is worthy of mentioning that the nomenclatures regarding Class I-III reactions are given by Rhines for three different types of invariant reactions in a ternary system,[36] which are also known as eutectic, quasi-peritectic (or U-reaction) and peritectic reactions, respectively. Moreover, there are two saddle points located along (Sb)/SnSe and SnSe/$Sn_2Sb_9Se_9$ univariant lines, respectively. It needs mentioning that the method adopted in this study is determination of the univariant lines based on the results of the determined primary solidification phases. No efforts are made to distinguish the same primary solidification phase but resulted from two different liquid phases in the miscibility gap. The invariant reactions involving two liquid phases are thus not determined in this study.

C. *673.2 K (400 °C) Sb-Se-Sn Phase Equilibria Isothermal Section*

To determine the 673.2 K (400 °C) Sb-Se-Sn isothermal section, sixteen Sb-Se-Sn alloys were prepared, and their nominal composition are listed in the Table III. Figures 7(a) and (b) Sb-Se-Sn isothermal sections at 673.2 K (400 °C) with and without superimpositions of the sixteen Sb-Se-Sn ternary alloys.

Figure 8(a) shows the BEI micrograph of alloy #47 (Sn-30.0 at. pct Sb-10.0 at. pct Se), and the three different phases, which are dark platy, bright bulk, and gray matrix phases, can be observed. The composition of platy and bulk phases are Sn-49.3 at. pct Se, and Sn-54.3 at. pct Sb-1.3 at. pct Se which can be determined as SnSe and SbSn phases. Along the Sn-Sb binary side,[21] there is a large liquid phase regime near Sn-rich corner. According to the Sn-Se binary phase diagram, there is a relatively small liquid phase regime and a big Liquid + SnSe two phase regime.[22] Based on the above results, the multiphase regime is probably the liquid phase at 673.2 K (400 °C). It is concluded that gray matrix with average composition of Sn-11.2 at. pct

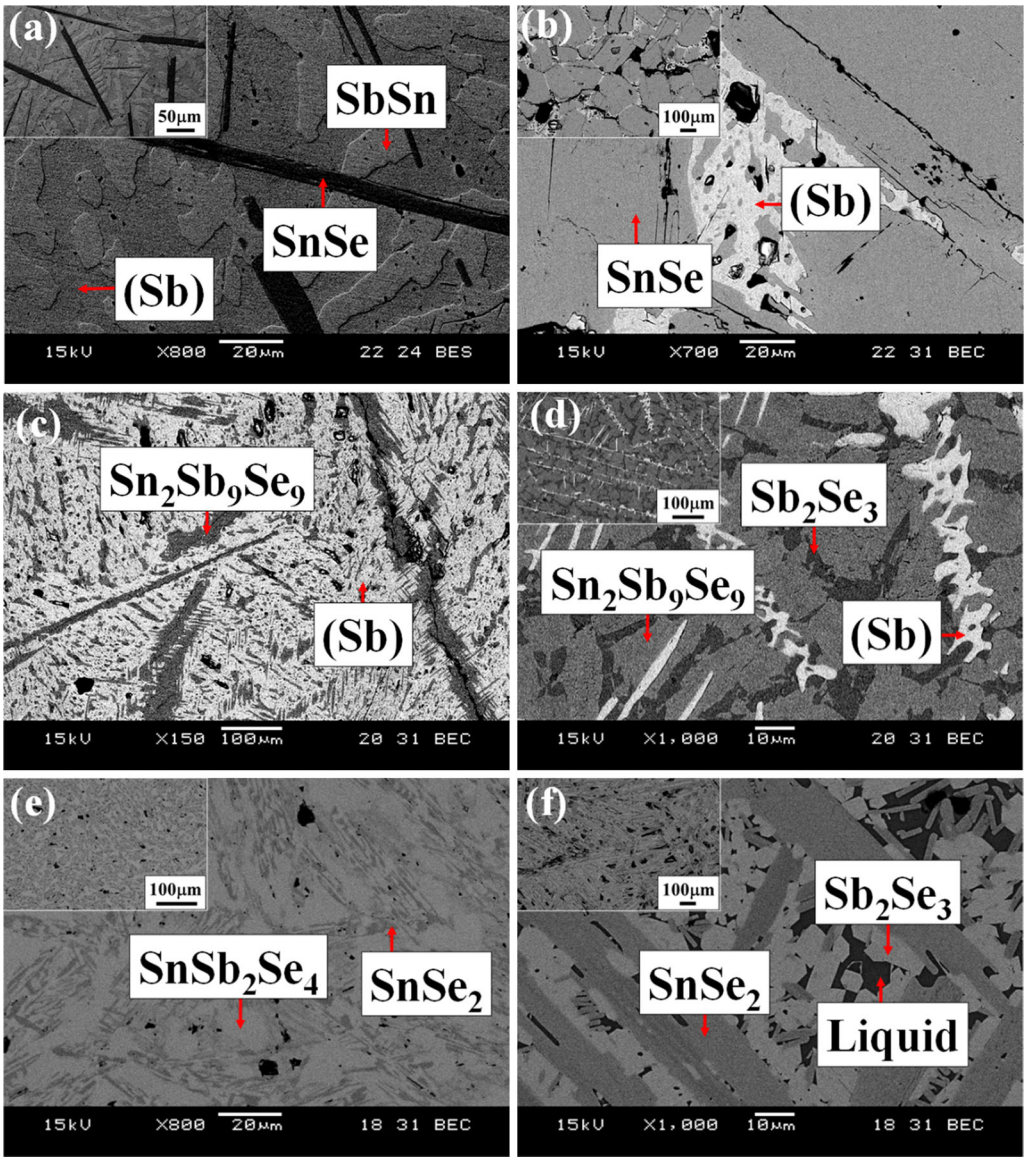

Fig. 10—(*a*) The BEI micrograph of equilibrated alloy #48 (Sn-30.0 at. pct Sb-30.0 at. pct Se). (*b*) The BEI micrograph of equilibrated alloy #50 (Sn-20.0 at. pct Sb-40.0 at. pct Se). (*c*) The BEI micrograph of equilibrated alloy #54 (Sn-75.0 at. pct Sb-20.0 at. pct Se). (*d*) The BEI micrograph of equilibrated alloy #56 (Sn-55.0 at. pct Sb-40.0 at. pct Se). (*e*) The BEI micrograph of equilibrated alloy #57 (Sn-20.0 at. pct Sb-60.0 at. pct Se). (*f*) The BEI micrograph of equilibrated alloy #58 (Sn-10.0 at. pct Sb-70.0 at. pct Se).

Sb-0.1 at. pct Se was the liquid phase prior to its removal from the furnace. Figure 8(b) shows the XRD diffractogram of alloy #47, the diffraction peaks of SnSe, SbSn, and (Sn) can be found, which agree with the results of micrographic and compositional analysis. It is concluded that alloy #47 is located at the SnSe + SbSn + Liquid three-phase region. Following similar procedures, it is determined that alloy #44 (Sn-10.0 at. pct Sb- 10.0 at. pct Se)–#46 (Sn-20.0 at. pct Sb-10.0 at. pct Se) are also located in the SnSe + SbSn + Liquid three-phase region.

Figure 9(a) shows the BEI micrograph of the alloy #52 (Sn-70.0 at. pct Sb-20.0 at. pct Se). The micrograph shows there are only two different phases. However, according to the elemental mapping of alloy #52 as shown in Figure 9(b), there are three different phases, dendritic, small rod-shaped and bright matrix phases. The compositional analysis of three phases were measured based on the results of elemental mapping, and the compositions of three phases are Sn-1.7. at. pct Sb-49.8 at. pct Se, Sn-42.1 at. pct Sb-45.2 at. pct Se, and Sn-98.6 at. pct Sb-0.2. at. pct Se, which are SnSe, $Sn_2Sb_9Se_9$, and (Sb) phases, respectively. The fact that there is extremely close contrast between the SnSe and $Sn_2Sb_9Se_9$ phases is attributed to the similar atomic numbers between Sn and Sb elements so that the average atomic numbers of SnSe and $Sn_2Sb_9Se_9$ are very close to each other. Figure 9(c) shows the XRD diffractogram of alloy #52, in which the diffraction peaks of SnSe, $Sn_2Sb_9Se_9$, and (Sb) can be identified.

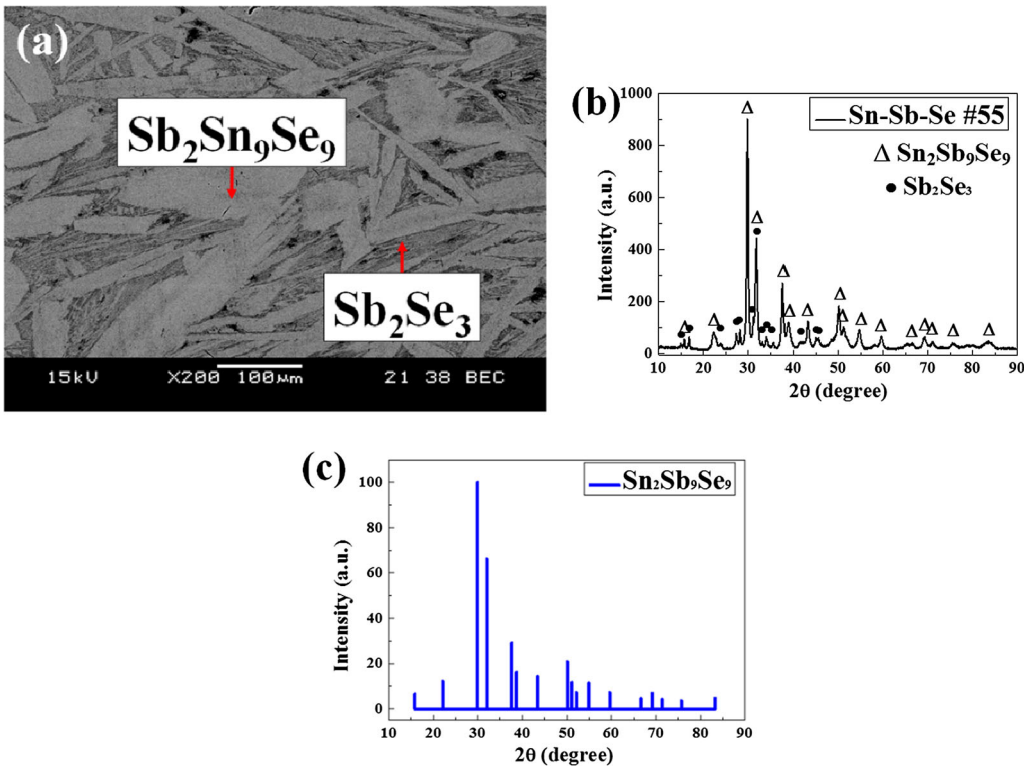

Fig. 11—(*a*) The BEI micrograph of equilibrated alloy #55 (Sn-45.0 at. pct Sb-50.0 at. pct Se). (*b*) The XRD diffractogram of equilibrated alloy #55. (*c*) The derived X-ray diffractogram of $Sn_2Sb_9Se_9$ ternary phase.

Table IV. The Information of the XRD Diffraction Peaks of $Sn_2Sb_9Se_9$ Phase

Diffraction angle (Deg)	Relative Intensity (Pct)	Diffraction Angle (Deg)	Relative Intensity (Pct)
15.9	7	52.1	7
22.1	12	54.9	11
29.9	100	59.6	7
32	66	66.6	5
37.6	29	69.2	7
38.7	16	71.4	4
43.4	14	75.7	4
50.1	21	83.3	5
51.1	12		

According to the above-mentioned results, the alloy #52 is located in the SnSe + $Sn_2Sb_9Se_9$ + (Sb) three-phase region.

Figures 10(a) through (f) show the BEI micrographs of yje alloys #48 (Sn-30.0 at. pct Sb-30.0 at. pct Se), #50 (Sn-20.0 at. pct Sb-40.0 at. pct Se), #54 (Sn-75.0 at. pct Sb-20.0 at. pct Se), #56 (Sn-55.0 at. pct Sb-40.0 at. pct Se), #57 (Sn-20.0 at. pct Sb-60.0 at. pct Se), and #58 (Sn-10.0 at. pct Sb-70.0 at. pct Se). Following similar procedures, the equilibrium phases can be determined, and they are in the SnSe + SbSn + (Sb), SnSe + (Sb), $Sn_2Sb_9Se_9$ + (Sb), $Sn_2Sb_9Se_9$ + (Sb) + Sb_2Se_3, $SnSe_2$ + $SnSb_2Se_4$, and $SnSe_2$ + Sb_2Se_3 + Liquid phase regions.

To determine the 673.2 K (400 °C) isothermal section of the Sb-Se-Sn ternary system, the information of binary boundaries along Sn-Sb, Sn-Se, and Sb-Se sides can be obtained by the three constituent binary systems.[21–23] Along the Sn-Sb side, the phase boundaries of Liquid/Liquid + SbSn, SbSn + Liquid/SbSn, SbSn/SbSn + (Sb), and SbSn + (Sb)/(Sb) are Sn-38.0 at. pct Sb, Sn-56.0.at. pct Sb, Sn-61.0 at. pct Sb, and Sn-87.5 at. pct Sb, respectively.[21] According to the Sn-Se binary phase diagram, the boundaries along Sn-Se side are Sn-50.0 at. pct Se, Sn-66.7 at. pct Se, and Sn-99.0 at. pct Se for SnSe/SnSe + $SnSe_2$, SnSe + $SnSe_2$/$SnSe_2$, and $SnSe_2$ + Liquid/Liquid.[22] Since there is low Se solubility in the (Sn) phase, the boundary between SnSe + Liquid/Liquid is hard to recognize.[22] Along the Sb-Se side, the phase boundaries are Sb-0.1 at. pct Se, Sb-60.0 at. pct Se, and Sb-96.0 at. pct Se for (Sb)/(Sb) + Sb_2Se_3, Sb_2Sb_3 + (Sb)/Sb_2Se_3 and Sb_2Se_3 + Liquid/Liquid, respectively.[23]

Figure 7(b) shows the 673.2 K (400 °C) isothermal section of Sb-Se-Sn ternary system, and the compositions of equilibrium phases are listed in Table III. In the 673.2 K (400 °C) isothermal section of Sb-Se-Sn ternary

system, there are nine tie triangles, which are Liquid + SnSe + SbSn, SnSe + SbSn + (Sb), SnSe + $Sn_2Sb_9Se_9$ + (Sb), $Sn_2Sb_9Se_9$ + (Sb) + Sb_2Se_3, SnSe + $Sn_2Sb_9Se_9$ + $SnSb_2Se_4$, $Sn_2Sb_9Se_9$ + $SnSb_2Se_4$ + Sb_2Se_3, SnSe + $SnSe_2$ + $SnSb_2Se_4$, $SnSe_2$ + $Sn_2Sb_9Se_9$ + $SnSb_2Se_4$, and $SnSe_2$ + Sb_2Se_3 + Liquid, respectively.

D. *The New Ternary Compound $Sn_2Sb_9Se_9$*

The nominal composition of alloy #55 (Sn-40.0 at. pct Sb-50.0 at. pct Se) is as same as the as-solidified alloy #36, but alloy #55 are annealed at 673.2 K (400 °C) for six months. Figure 11(a) shows the BEI micrograph of alloy #55, two phases, which are gray bulk and dark matrix phases can be observed from the microstructure. It is worthy of mentioning that gray bulk phase occupied almost 80 pct of microstructure of alloy #55. The composition of the equilibrium phases are Sn-41.5 at. pct Sb-45.0 at. pct Se and Sn-41.0 at. pct Sb-58.8 at. pct Se, which can be determined as possible new ternary phase, $Sn_2Sb_9Se_9$ and Sb_2Se_3 phase. Compared with the micrograph of alloy #36 as shown in Figure 4(b), the $Sn_2Sb_9Se_9$ ternary phase obviously grows larger with longer annealed time. Figure 11(b) shows the XRD diffractogram of alloy #55, where the diffraction patterns of $Sn_2Sb_9Se_9$ and Sb_2Se_3 phases are found. Figure 11(c) shows the diffraction pattern of the $Sn_2Sb_9Se_9$ phase which is determined by extracting the peaks of Sb_2Se_3 phase. The detailed information of the XRD diffraction peaks of $Sn_2Sb_9Se_9$ phase is summarized in the Table IV. Since the $Sn_2Sb_9Se_9$ ternary phase is the newly founded phase in this study, further analysis should be investigated in the future.

IV. CONCLUSIONS

The liquidus projection and 673.2 K (400 °C) isothermal section of the Sb-Se-Sn ternary system are experimentally determined in this study. There are ten primary solidification phases: (Sn), (Sb), (Se), Sb_2Sn_3, SbSn, Sb_2Se_3, SnSe, $SnSe_2$, $Sn_2Sb_9Se_9$, and $SnSb_2Se_4$ phases, in the liquidus projection. There are ten ternary invariant reactions involving liquid in the 673.2 K (400 °C) isothermal section of Sb-Se-Sn ternary system, and there are nine tie-triangles: Liquid + SnSe + SbSn, SnSe + SbSn + (Sb), SnSe + $Sn_2Sb_9Se_9$ + (Sb), $Sn_2Sb_9Se_9$ + (Sb) + Sb_2Se_3, SnSe + $Sn_2Sb_9Se_9$ + $SnSb_2Se_4$, $Sn_2Sb_9Se_9$ + $SnSb_2Se_4$ + Sb_2Se_3, SnSe + $SnSe_2$ + $SnSb_2Se_4$, $SnSe_2$ + $Sn_2Sb_9Se_9$ + $SnSb_2Se_4$, and $SnSe_2$ + Sb_2Se_3 + Liquid. In addition, the possible new ternary compound, $Sn_2Sb_9Se_9$, was found for the first time in this study.

ACKNOWLEDGMENT

This study is financially sponsored by the National Science Council of Taiwan (NSC 103-2923-E-007-002-MY2).

REFERENCES

1. T. Nishida, H. Sugiyama, and S. Horigome: *Jpn. J. Appl. Phys.*, 1995, vol. 34 (3), pp. 1562–68.
2. P. Kumar and R. Thangaraj: *J. Non-Cryst. Solids*, 2006, vol. 352, pp. 2288–91.
3. P. Kumar, J. Kumar, M. Ahmad, and R. Thangaraj: *Appl. Phys. A*, 2008, vol. 90 (3), pp. 469–73.
4. M. Ahmad, P. Kumar, and R. Thangaraj: *Thin Solid Films*, 2009, vol. 517, pp. 5965–68.
5. P. Kumar, R. Thangaraj, and T.S. Sathiaraj: *J. Non-Cryst. Solids*, 2010, vol. 356, pp. 1611–13.
6. M. Ahmad, R. Thangaraj, and T. Stephen Sathiaraj: *J. Mater. Sci.*, 2010, vol. 45 (5), pp. 1231–36.
7. R. Chander and R. Thangaraj: *Appl. Phys. A*, 2010, vol. 99 (1), pp. 181–87.
8. M.T.S. Nair, E.B. Salgado, A.R. García, M.R.A. Silva, J. Campos, and P.K. Nair: *ECS Trans.*, 2011, vol. 41, pp. 177–83.
9. R. Chander and R. Thangaraj: *Thin Solid Films*, 2012, vol. 520 (6), pp. 1757–61.
10. R. Chander and R. Thangaraj: *Appl. Phys. A*, 2014, vol. 114 (2), pp. 619–24.
11. F.M.A. Rahim and K.A. Aly: *J. Non-Cryst. Solid*, 2015, vol. 419, pp. 69–74.
12. T.R. Wei, H. Wang, Z.M. Gibbs, C.F. Wu, G.F. Snyder, and J.F. Li: *J. Mater. Chem. A*, 2014, vol. 2, pp. 13527–33.
13. M. Tsega, D.H. Kuo, and F.B. Dejene: *Thin Solid Films*, 2015, vol. 589, pp. 712–17.
14. C.E. Patrick and F. Giustino: *Adv. Funct. Mater.*, 2011, vol. 21 (24), pp. 4663–67.
15. N. Guijarro, T. Lutz, T.L. Villarreal, F. O'Mahony, R. Gómez, and S.A. Haque: *J. Phys. Chem. Lett.*, 2012, vol. 3 (10), pp. 1351–56.
16. J.H. Rhee, C.C. Chung, and E.W.G. Diau: *NPG Asia Mater.*, 2013, vol. 5, p. e68.
17. M.A. Franzman, C.W. Schlenker, M.E. Thompson, and R.L. Brutchey: *J. Am. Chem. Soc.*, 2010, vol. 132, pp. 4060–61.
18. X. Yu, J. Zhu, Y. Zhang, J. Weng, L. Hu, and S. Dai: *Chem. Commun.*, 2012, vol. 48, pp. 3324–26.
19. M. Wobst: *J. Less Common Met.*, 1968, vol. 14, pp. 77–81.
20. M.A. Alidzhanov, M.Z. Alizade, and A.P. Gurshumov: *Inorg. Mater.*, 1985, vol. 21, pp. 1285–87.
21. H. Okamoto: *J. Phase Equilib. Diff.*, 2012, vol. 33, p. 347.
22. H. Okamoto: *J. Phase Equilib.*, 1998, vol. 19, p. 293.
23. H. Okamoto:, in *Binary Alloy Phase Diagrams*, T.B. Massalski, H. Okamoto, P.R. Subramanian, and L. Kacprzak, eds., ASM International, Ohio, 1990, pp. 3300–02.
24. P.G. Harrison and P. Hubberstey:Elements of group V, in *Inorganic Chemistry of the Main-Group Elements*, C.C. Addison, ed., Royal Society of Chemistry, London, 1977.
25. P.P.K. Smith and J.B. Parise: *Acta Cryst.*, 1985, vol. B41, pp. 84–87.
26. J. Shen and R. Blachnik: *Thermochim. Acta*, 2003, vol. 399, pp. 245–46.
27. I. Trabelsi, N. Ben Mehrez, and M. Kanzari: *J. Mater. Sci: Mater. Electron.*, 2015, vol. 26 (10), pp. 7763–70.
28. P.E.J. Flewitt and R.K. Wild: *Physical Methods for Materials Characterization*, Institute of Physics Publishing, Bristol, 1994.
29. J.S. Chang, K.C. Chiu, S.W. Chen, H.J. Wu, and J.J. Chen: *Metall. Mater. Trans. A*, 2014, vol. 45A, pp. 3728–40.
30. J.S. Chang and S.W. Chen: *J. Electron. Mater.*, 2014, vol. 44 (4), pp. 1134–43.
31. S.W. Chen, J.S. Chang, S.M. Tseng, L.C. Chang, and J.Y. Lin: *J. Alloy. Compd.*, 2015, vol. 656, pp. 58–66.
32. J.S. Chang and S.W. Chen: *J. Alloy. Compd.*, 2016, vol. 666, pp. 159–69.
33. S.W. Chen, C.C. Huang, and J.C. Lin: *Chem. Eng. Sci.*, 1995, vol. 50, pp. 417–31.
34. S.C. Jeng and S.W. Chen: *Acta Mater.*, 1997, vol. 45, pp. 4887–99.
35. W.J. Boettinger, U.R. Kattner, K.-W. Moon, and J.H. Perepezko: *DTA and DSC Heat Flux Measurements of Alloy Melting and Freezing*, NIST, Washington DC, 2006.
36. F.N. Rhines: *Phase Diagram in Metallurgy: Their Development and Application*, McGraw-Hill, New York, 1956.